Through-the-Wall Human Motion Indication Using Sparsity-Driven Change Detection

Fauzia Ahmad, *Senior Member, IEEE*, and Moeness G. Amin, *Fellow, IEEE*

***Abstract*—We consider sparsity-driven change detection (CD) for human motion indication in through-the-wall radar imaging and urban sensing applications. Stationary targets and clutter are removed via CD, which converts a populated scene into a sparse scene of a few human targets moving inside enclosed structures and behind walls. We establish appropriate CD models for various possible human motions, ranging from translational motions to sudden short movements of the limbs, head, and/or torso. These models permit scene reconstruction within the compressive sensing framework. Results based on laboratory experiments show that a sizable reduction in the data volume is achieved using the proposed approach without a degradation in system performance.**

***Index Terms*—Change detection (CD), compressive sensing (CS), sparse reconstruction, through-the-wall radar.**

I. Introduction

One of the primary objectives in through-the-wall radar imaging (TWRI) and urban sensing is the detection and localization of human targets [1]–[7]. Humans belong to the class of animate objects, which is characterized by motion of the body, breathing, and heartbeat. These features make animate objects distinguishable from inanimate objects and allow the detection of targets of interest to proceed based on changes in the phase of the scattered radar signals over successive probing and data observations.

For urban sensing environments, changes in the backscattered signal phase due to human motion do not necessarily lend themselves to Doppler frequency shifts. This is because the human motion can be abrupt and highly nonstationary, producing a time-dependent phase whose rate of change may fail to translate into a single Doppler shift or multi-component sinusoids that can be captured by different Doppler filters. Instead, the corresponding wide spectrum of human motions becomes nonlocalizable and can span the entire radar frequency band. In lieu of Doppler filters, time-frequency processing can be applied to reveal the instantaneous frequency signatures [8]–[10]. However, apart from regularized motions, such as walking and running, time-frequency Doppler signal representations are often very complex and difficult to interpret, particularly when dealing with non-homogeneous walls. Therefore, the application of Doppler and micro-Doppler filters for indoor target surveillance may not be a viable option.

Change detection (CD) can be used in lieu of Doppler processing, wherein human detection is accomplished by subtraction of data frames acquired over successive probing of the scene. CD in TWRI has been discussed in the recent literature, both in the context of moving target indication [3], [11]–[15] and background subtraction to detect stationary targets using data acquired during interrogations of a scene at two different time instants [15], [16]. Target detection in through-the-wall radar applications is, in general, a very challenging problem, given the level of multipath and clutter that can contaminate the radar image and the overwhelming return from the front wall that tends to obscure the nearby indoor targets. For stationary target detection, CD requires availability of a reference (background) data set without the targets, which is very difficult to obtain in practice. Target motion, on the other hand, allows easy access to a reference data set through multiple interrogations of the scene.

For moving targets, CD mitigates the heavy clutter that is caused by strong reflections from exterior and interior walls and also removes stationary objects present in the enclosed structure, thereby rendering a densely populated scene sparse [3], [14], [17]. As a result, it becomes possible and more convenient to exploit compression in data collections and processing. Efficient data acquisition and processing enable achieving situational awareness in a quick and reliable manner, which is highly desirable in TWRI and urban sensing applications. The capability of the emerging compressive sensing (CS) techniques to reconstruct a sparse signal from far fewer nonadaptive measurements provides a new perspective for data reduction in radar imaging without compromising the imaging quality [18]–[21]. The application of CS for TWRI was first reported in [22]. CS techniques can improve the efficacy of the urban sensing operations by reducing the number of antenna elements and/or the number of time samples or frequency steps, depending on the choice of the transmit waveform, culminating in quick turnaround, reliable, and actionable intelligence [22]–[24].

In this paper, we consider sparsity-based CD in imaging radar systems, aiming at detection and localization of human targets inside buildings, while simultaneously achieving a sizable reduction in the data volume. CD is first used for stationary background removal. Rather than operating on successive pulses, CD is applied to different data frames for each range bin in the unambiguous range. It is noted that the frames can be consecutive, dealing with targets exhibiting sudden short motions, or nonconsecutive, with relatively long time difference, for the

Manuscript received December 20, 2011; revised March 20, 2012; accepted May 6, 2012. Date of publication July 23, 2012; date of current version January 17, 2013. This work was supported in part by the Office of Naval Research under Grant N00014-11-1-0576 and in part by Army Research Office and Army Research Laboratory under contract W911NF-11-1-0536.

The authors are with the Radar Imaging Lab, Center for Advanced Communications, Villanova University, Villanova, PA 19085 USA (e-mail: fauzia.ahmad@villanova.edu; moeness.amin@villanova.edu).

Color versions of one or more of the figures in this paper are available online at http://ieeexplore.ieee.org.

Digital Object Identifier 10.1109/TGRS.2012.2203310

case in which the target changes its range gate position. Scene reconstruction is then achieved using sparsity-driven imaging. We focus on human targets undergoing translational motion as well as sudden short movements of their limbs, heads, and/or torsos. The latter is a typical situation underlying the activities in homes, lecture halls, and auditoriums as well as other sit-down human interactions. For each type of motion, we establish an appropriate CD model that permits formulation of linear modeling with sensing matrices, so as to apply CS for scene reconstruction.

Supporting examples based on real data collected in a laboratory environment, using the Radar Imaging Facility at the Center for Advanced Communications, Villanova University, are provided. We use an imaging system with a physical aperture. Single target sparse scenes are imaged with the human undergoing both translation and short sudden movement of the head. For both types of human motions, it is shown that, compared to the conventional back projection-based CD, the sparsity-driven CD achieves substantial reduction in the data volume without any degradation in the system performance. The scene reconstructions obtained with the sparsity-based CD not only accurately localize the target undergoing motion, but are also far less cluttered than the conventional reconstructions.

The paper is organized as follows. In Section II, we describe the signal model and CD for conventional back projection-based scene reconstruction. We discuss the sparsity-driven CD schemes under translational and abrupt human motions in Sections III and IV, respectively, highlighting the key equations. Section V presents experimental results, comparing the performance of back projection-based CD and sparsity-based CD using real data of human motion behind a cement board wall. Section VI contains the conclusions.

II. Backprojection-Based Change Detection

We first develop the signal model for wideband radar operation with M transmitters and N receivers. A sequential multiplexing of the transmitters with simultaneous reception at multiple receivers is assumed. Although this signaling approach demands more acquisition time compared to the simultaneous transmitter operation, it is a viable option for TWRI operations. This is because 1) more receivers than transmitters are deployed due to the important constraint of low cost, and 2) the targets of interest move at low velocities indoors. As a result, loss of coherence of the target response may not be an issue. It is important to note that the sequential transmit operation is the salient feature of three known TWRI systems; one is built by the Army Research Lab [3], [25], the other by the Defense Research and Development Canada [26], and the third by MIT Lincoln Lab [13]. With the assumption of sequential multiplexing, a signal model can thus be developed based on single active transmitters. We note that the timing interval for each data frame is assumed to be a fraction of a second so that the moving target appears stationary during each data collection interval.

Let $s(t)$ be the wideband base band signal used for interrogating the scene. For the case of a single point target, located at $\mathbf{x}_p = (x_p, y_p)$, the pulse emitted by the mth transmitter with phase center at $\mathbf{x}_{tm} = (x_{tm}, 0)$ is received at the nth receiver with phase center at $\mathbf{x}_{rn} = (x_{rn}, 0)$ in the form

$$\begin{aligned} z_{mn}(t) &= a_{mn}(t) + b_{mn}(t) \\ a_{mn}(t) &= \sigma_p s(t - \tau_{p,mn}) \exp(-j\omega_c \tau_{p,mn}) \end{aligned} \tag{1}$$

where σ_p is the complex reflectivity of the target, which is assumed to be independent of frequency and aspect angle, ω_c is the carrier frequency, $\tau_{p,mn}$ is the propagation delay for the signal to travel between the mth transmitter, the target at $\mathbf{x}_p$, and the nth receiver, and $b_{mn}(t)$ represents the contribution of the stationary background at the nth receiver with the mth transmitter active. For through-the-wall propagation, $\tau_{p,mn}$ will comprise the components corresponding to traveling distances before, through, and after the wall [27], [28]. Note that the expression in (1) does not consider the wall attenuation and free-space path loss encountered by the radar return. In case of two targets of equal reflectivity located at different distances from the radar system, these losses cause the distant target to appear weaker than the closer target in the image. The wall attenuation and path loss can be easily accommodated in (1) through the use of a scaling factor [20]. However, for notational convenience, we chose to ignore these losses in the problem formulation.

In its simplest form, CD is achieved by coherent subtraction of the data corresponding to two data frames, which may be consecutive or separated by one or more data frames. This subtraction operation is performed for each range bin. CD results in the set of difference signals, given by

$$\delta z_{mn}(t) = z_{mn}^{(L+1)}(t) - z_{mn}^{(1)}(t) = a_{mn}^{(L+1)}(t) - a_{mn}^{(1)}(t) \tag{2}$$

where L denotes the number of frames between the two time acquisitions. The component of the radar return from the stationary background is the same over the two time intervals, and is thus removed from the difference signal. We assume that the clutter bandwidth is zero, and it is confined to the zero Doppler frequency. It is noted that $L = 1$ represents the case when the two acquisitions are performed over consecutive frames. Using (1) and (2), the (m, n)-th difference signal can be expressed as

$$\begin{aligned} \delta z_{mn}(t) = \sigma_p s\left(t - \tau_{p,mn}^{(L+1)}\right) \exp\left(-j\omega_c \tau_{p,mn}^{(L+1)}\right) \\ - \sigma_p s\left(t - \tau_{p,mn}^{(1)}\right) \exp\left(-j\omega_c \tau_{p,mn}^{(1)}\right) \end{aligned} \tag{3}$$

where $\tau_{p,mn}^{(1)}$ and $\tau_{p,mn}^{(L+1)}$ are the respective two-way propagation delays for the signal to travel between the mth transmitter, the target, and the nth receiver, during the first and the second data acquisitions, respectively.

In order to generate an image of the scene being interrogated, the MN difference signals corresponding to the operation of M transmitters and N receivers are processed as follows. The region of interest is divided into a finite number of grid points in x and y, where x and y represent cross range and downrange, respectively. The composite signal corresponding to the pixel,

located at $\mathbf{x}_q = (x_q, y_q)$, is obtained by summing time delayed versions of the MN difference signals

$$\begin{aligned}\delta z_q(t) &= \sum_{m=0}^{M-1}\sum_{n=0}^{N-1} \delta z_{mn}(t+\tau_{q,mn}) \\ &= \sum_{m=0}^{M-1}\sum_{n=0}^{N-1} \left(a_{mn}^{(L+1)}(t+\tau_{q,mn}) - a_{mn}^{(1)}(t+\tau_{q,mn})\right) \quad (4)\end{aligned}$$

where $\tau_{q,mn}$ is the focusing delay applied to the (m,n)th difference signal. It is noted that additional weighting can be applied during the summation operations of (4) to control the sidelobe level of the system point spread function [27], [28]. Substituting from (3) in (4) yields

$$\begin{aligned}\delta z_q(t) = \sum_{m=0}^{M-1}\sum_{n=0}^{N-1} \sigma_p \Big(& s\left(t+\tau_{q,mn}-\tau_{p,mn}^{(L+1)}\right) \\ & \times \exp\left(-j\omega_c\left(\tau_{p,mn}^{(L+1)} - \tau_{q,mn}\right)\right) \\ & - s\left(t+\tau_{q,mn}-\tau_{p,mn}^{(1)}\right) \\ & \times \exp\left(-j\omega_c\left(\tau_{p,mn}^{(1)} - \tau_{q,mn}\right)\right)\Big). \quad (5)\end{aligned}$$

The complex amplitude image value $I(\mathbf{x}_q)$ for the pixel at $\mathbf{x}_q$ is then obtained by applying a filter, matched to $s(t)$, to $\delta z_q(t)$ and sampling the filtered data, as per the following equation:

$$I(\mathbf{x}_q) = \delta z_q(t) * h(t)\big|_{t=0} \quad (6)$$

where $h(t) = s^*(-t)$ is the impulse response of the matched filter, the superscript "$*$" denotes complex conjugation, and "$*$" denotes the convolution operator. The process described by (4)–(6) is repeated for all pixels in the image to generate the composite image of the scene. The general case of multiple targets can be obtained by superposition of target reflections [27], [28].

Normally, we work with discrete versions of the measured time signals. Note that not all time samples of the difference signal are necessary to obtain the corresponding image. Even if some of the data samples are missing, information on the moving targets in the field of view can still be obtained. However, merely employing part of the signal time duration in back projection provides an image quality that is degraded in proportion to the number of missing data [29]. Since the removal of stationary background converts a populated scene into a sparse scene of moving targets, reduction in data volume should be pursued under the CS framework.

III. Sparsity-Driven Change Detection Under Translational Motion

Consider the difference signal in (3), reproduced below for convenience, for the case where the target is undergoing translational motion. Two nonconsecutive data frames with relatively long time difference are used, i.e., $L \gg 1$

$$\begin{aligned}\delta z_{mn}(t) = \sigma_p s\left(t-\tau_{p,mn}^{(L+1)}\right)\exp\left(-j\omega_c\tau_{p,mn}^{(L+1)}\right) \\ - \sigma_p s\left(t-\tau_{p,mn}^{(1)}\right)\exp\left(-j\omega_c\tau_{p,mn}^{(1)}\right). \quad (7)\end{aligned}$$

In this case, the target will change its range gate position during the time elapsed between the two data acquisitions. As seen from (7), the moving target will present itself as two targets, one corresponding to the target position during the first time interval, and the other corresponding to the target location during the second data frame. It is noted that the imaged target at the reference position corresponding to the first data frame cannot be suppressed for the coherent CD approach, whether employing back projection or sparsity-driven imaging. On the other hand, the noncoherent CD approach that deals with differences of image magnitudes corresponding to the two data frames, allows suppression of the reference image through a zero thresholding operation [14]. However, as the noncoherent approach requires the scene reconstruction to be performed prior to CD, it is not a feasible option for sparsity-based imaging, which relies on coherent CD to render the scene sparse. Therefore, we rewrite (7) as

$$\delta z_{mn}(t) = \sum_{i=1}^{2} \widetilde{\sigma}_i s(t-\tau_{i,mn})\exp(-j\omega_c\tau_{i,mn}) \quad (8)$$

with

$$\widetilde{\sigma}_i = \begin{cases}\sigma_p & i=1 \\ -\sigma_p & i=2\end{cases}$$

$$\tau_{i,mn} = \begin{cases}\tau_{p,mn}^{(L+1)} & i=1 \\ \tau_{p,mn}^{(1)} & i=2.\end{cases} \quad (9)$$

Assume that the scene being imaged, or the target space, is divided into a finite number of grid points in cross range and downrange. If we sample the difference signal $\delta z_{mn}(t)$ at times $\{t_k\}_{k=0}^{K-1}$ to obtain the $K \times 1$ vector $\mathbf{\Delta z}_{mn}$ and form the concatenated $Q \times 1$ scene reflectivity vector $\widetilde{\boldsymbol{\sigma}}$ corresponding to the spatial sampling grid, then using the developed signal model in (9), we obtain the linear system of equations [20], [22], [24]

$$\mathbf{\Delta z}_{mn} = \mathbf{\Psi}_{mn}\widetilde{\boldsymbol{\sigma}}. \quad (10)$$

The qth column of $\mathbf{\Psi}_{mn}$ consists of the received signal corresponding to a target at grid point $\mathbf{x}_q$ and the kth element of the qth column can be written as [20]

$$\begin{aligned}[\mathbf{\Psi}_{mn}]_{k,q} = \frac{s(t_k-\tau_{q,mn})\exp(-j\omega_c\tau_{q,mn})}{\|\mathbf{s}_{q,mn}\|_2} \\ k=0,1,\ldots,K-1, \quad q=0,1,\ldots,Q-1 \quad (11)\end{aligned}$$

where $\tau_{q,mn}$ is the two-way signal traveling time from the mth transmitter to the qth grid point and back to the nth receiver. Note that the kth element of the vector $\mathbf{s}_{q,mn}$ is $s(t_k - \tau_{q,mn})$, which implies that the denominator in the R.H.S. of (11) is the energy in the time signal. Therefore, each column of $\mathbf{\Psi}_{mn}$ has unit norm. Further note that $\widetilde{\boldsymbol{\sigma}}$ in (10) is a weighted indicator vector defining the scene reflectivity, i.e., if there is a target at the qth grid point, the value of the qth element of $\widetilde{\boldsymbol{\sigma}}$ should be $\widetilde{\sigma}_q$; otherwise, it is zero.

The CD model described in (10) and (11) permits the scene reconstruction within the CS framework. We measure an

$L(< K)$ dimensional vector of elements randomly chosen from $\mathbf{\Delta z}_{mn}$. The new measurements can be expressed as

$$\boldsymbol{\xi}_{mn} = \mathbf{\Phi}_{mn}\mathbf{\Delta z}_{mn} = \mathbf{\Phi}_{mn}\mathbf{\Psi}_{mn}\widetilde{\boldsymbol{\sigma}} \tag{12}$$

where $\mathbf{\Phi}_{mn}$ is an $L \times K$ measurement matrix. Several types of measurement matrices have been reported in the literature [20], [21], [30 and the references therein]. To name a few, a measurement matrix whose elements are drawn from a Gaussian distribution, a measurement matrix having random ± 1 entries with probability of 0.5, or a random matrix whose entries can be constructed by randomly selecting rows of a $K \times K$ identity matrix. It was shown in [20] that the measurement matrix with random ± 1 elements requires the least amount of compressive measurements for the same radar imaging performance and permits a relatively straight forward data acquisition implementation. Therefore, we choose to use such a measurement matrix in image reconstructions.

Given $\boldsymbol{\xi}_{mn}$ for $m = 0, 1, \ldots, M-1$, $n = 0, 1, \ldots, N-1$, we can recover $\widetilde{\boldsymbol{\sigma}}$ by solving the following equation:

$$\hat{\widetilde{\boldsymbol{\sigma}}} = \arg\min_{\widetilde{\boldsymbol{\sigma}}} \|\widetilde{\boldsymbol{\sigma}}\|_{l_1} \quad \text{subject to} \quad \mathbf{\Phi\Psi}\widetilde{\boldsymbol{\sigma}} \approx \boldsymbol{\xi} \tag{13}$$

where

$$\begin{aligned} \mathbf{\Psi} &= \left[\mathbf{\Psi}_{00}^T\ \mathbf{\Psi}_{01}^T\ \cdots\ \mathbf{\Psi}_{(M-1)(N-1)}^T\right]^T \\ \mathbf{\Phi} &= \operatorname{diag}\left(\mathbf{\Phi}_{00}, \mathbf{\Phi}_{01}, \ldots, \mathbf{\Phi}_{(M-1)(N-1)}\right) \\ \boldsymbol{\xi} &= \left[\boldsymbol{\xi}_{00}^T\ \boldsymbol{\xi}_{01}^T\ \cdots\ \boldsymbol{\xi}_{(M-1)(N-1)}^T\right]^T. \end{aligned} \tag{14}$$

A stable solution of the sparse target space reconstruction problem in (13) is guaranteed provided that the product matrix $\mathbf{\Phi\Psi}$ satisfies the restricted isometry property (RIP), which states that all subsets of r columns taken from $\mathbf{\Phi\Psi}$ are, in fact, nearly orthogonal, r being the sparsity of the signal $\widetilde{\boldsymbol{\sigma}}$ [20], [21], [31]. A measurement matrix $\mathbf{\Phi}$, whose elements are independent, identically distributed Bernoulli or Gaussian random variables, has been shown to satisfy the RIP with matrix $\mathbf{\Psi}$ resulting from sinusoids, wavelets, Gabor functions, etc. [32]. In general, it is computationally difficult to check this property and, therefore, other related measures on the product matrix $\mathbf{\Phi\Psi}$, such as mutual coherence, are often used to guarantee stable recovery through l_1-minimization [21]. Mutual coherence of the columns of $\mathbf{\Phi\Psi}$ can be viewed as the largest off-diagonal entry of the Gram matrix $(\mathbf{\Phi\Psi})^H(\mathbf{\Phi\Psi})$, where the columns of $\mathbf{\Phi\Psi}$ have been normalized. The matrix $\mathbf{\Phi\Psi}$ is considered to be incoherent if the value of the mutual coherence is small. We will address the mutual coherence of the product matrix $\mathbf{\Phi\Psi}$ used in the experimental results in Section V. We note that the problem in (13) can be solved using convex relaxation, greedy pursuit, or combinatorial algorithms [31], [33], [34]. In this paper, we choose CoSaMP as the reconstruction algorithm primarily because of its ability to handle complex arithmetic [33].

Equations (13) and (14) represent one strategy that can be adopted for sparsity-based CD approach, wherein a reduced number of time samples are chosen randomly for all the transmitter-receiver pairs constituting the array apertures. The above two equations can also be extended so that the reduction in data measurements includes both spatial and time samples [20], [22]. The latter strategy is not considered in this paper.

IV. Sparsity-Driven Change Detection Under Short Sudden Movement

Assume that consecutive $(L = 1)$ data frames are employed for CD and consider a scene comprising a human target undergoing sudden short movements of the limbs, head, and/or torso. That is, only a small portion of the body moves but remains within the same resolution cell. In this case, we can model the target as a cluster of P point scatterers within the same resolution cell and only a small number, say P_1, of these scatterers moves during successive data acquisitions. For example, in a round-the-table meeting, the upper part of the human body, particularly the hands, is likely to move while the legs remain stationary over successive observations. Using (1), the base band received signal, corresponding to the (m, n)th transmitter-receiver pair, for the first data frame can be expressed as

$$z_{mn}^{(1)}(t) = \sum_{p=1}^{P} \sigma_p s\left(t - \tau_{p,mn}^{(1)}\right) \exp\left(-j\omega_c \tau_{p,mn}^{(1)}\right) + b_{mn}(t) \tag{15}$$

where σ_p is the complex reflectivity of the pth point scatterer, and $\tau_{p,mn}^{(1)}$ is the two-way propagation delay for the signal to travel between the (m, n)th transmitter-receiver pair and the pth scatterer during the first frame. As the P scatterers are clustered within the same resolution cell, we can rewrite (15) as

$$z_{mn}^{(1)}(t) = \sigma_{mn}^{(1)} s(t - \overline{\tau}_{mn}) \exp(-j\omega_c \overline{\tau}_{mn}) + b_{mn}(t) \tag{16}$$

where $\bar{\tau}_{mn}$ is the propagation delay from the mth transmitter to the center of the cell and back to the nth receiver, and

$$\sigma_{mn}^{(1)} = \sum_{p=1}^{P} \sigma_p \exp\left(-j\omega_c \Delta\tau_{p,mn}^{(1)}\right) \tag{17}$$

is the net target reflectivity with $\Delta\tau_{p,mn}^{(1)} = \tau_{p,mn}^{(1)} - \bar{\tau}_{mn}$.

Let the first P_1 scatterers represent the portion of the body that undergoes a short movement. Then, the (m, n)th received signal corresponding to the second data frame can be expressed as

$$z_{mn}^{(2)}(t) = \sigma_{mn}^{(2)} s(t - \overline{\tau}_{mn}) \exp(-j\omega_c \overline{\tau}_{mn}) + b_{mn}(t) \tag{18}$$

with the net reflectivity $\sigma_{mn}^{(2)}$ given by

$$\sigma_{mn}^{(2)} = \sum_{p=1}^{P_1} \sigma_p \exp\left(-j\omega_c \Delta\tau_{p,mn}^{(2)}\right) + \sum_{p=P_1+1}^{P} \sigma_p \exp\left(-j\omega_c \Delta\tau_{p,mn}^{(1)}\right) \tag{19}$$

and the set of differential delays, $\{\Delta\tau_{p,mn}^{(2)} = \tau_{p,mn}^{(2)} - \bar{\tau}_{mn}\}_{p=1}^{P_1}$, corresponds to the new locations of the P_1 scatterers within

the same resolution cell. The difference signal corresponding to these successive data measurements is given by

$$\begin{aligned}\delta z_{mn}(t) &= z_{mn}^{(2)}(t) - z_{mn}^{(1)}(t) \\ &= \left(\sigma_{mn}^{(2)} - \sigma_{mn}^{(1)}\right) s(t-\overline{\tau}_{mn}) \exp(-j\omega_c \overline{\tau}_{mn}) \\ &= \delta\sigma_{mn} s(t-\overline{\tau}_{mn}) \exp(-j\omega_c \overline{\tau}_{mn}) \end{aligned} \tag{20}$$

where $\delta\sigma_{mn}$ represents the change in reflectivity between the consecutive acquisitions.

Again, working with a discretized version of (20) and for the target space consisting of Q grid points in cross range and downrange, we obtain the linear system of equations

$$\boldsymbol{\Delta z}_{mn} = \boldsymbol{\Psi}_{mn} \boldsymbol{\delta\sigma}_{mn} \tag{21}$$

where $\boldsymbol{\Psi}_{mn}$ is defined in (11) and $\boldsymbol{\delta\sigma}_{mn}$ is a weighted indicator vector defining the change in scene reflectivity as observed at the nth receiver with the mth transmitter active, i.e., if there is a change in target reflectivity at the qth grid point, the value of the qth element of $\boldsymbol{\delta\sigma}_{mn}$ will be $\sigma_{q,mn}^{(2)} - \sigma_{q,mn}^{(1)}$ and zero otherwise.

For the signal model in (21), we observe that the change in scene reflectivity depends on the transmitter and receiver locations. As such, the aspect-independent scattering assumption is no longer applicable, and there exists a map of the change in scene reflectivity for each transmitter-receiver pair. To address this issue of limited persistence in the change in target reflectivity across the various transmit-receive pairs, we consider composite image formation using sub-apertures [35]. In this scheme, the transmit and receive arrays are divided into sub-apertures. Assuming isotropic scattering within the angular extent of these sub-apertures, sub-images can be obtained, which are then combined to form a single composite image of the scene. The sub-aperture based-scene reconstruction can be performed within the CS framework using the CD model of (21).

Assume the M-element transmit and the N-element receive arrays are divided into K_1 and K_2 non-overlapping sub-apertures, respectively. The choice of K_1 and K_2 is guided by the local isotropy requirement, i.e., each transmit and receive sub-aperture should correspond to a small aspect angle data set (typically on the order of a few degrees). In the spirit of CS, a small number of "random" measurements carry enough information to completely represent the sparse signal $\boldsymbol{\delta\sigma}^{(k_1,k_2)}$, which is the "image" of the scene corresponding to the k_1th transmit and the k_2th receive sub-apertures. Thus, we measure a random subset of $L(<K)$ samples of the difference signal for the n_{k_2} th antenna of the k_2th receive sub-aperture when the m_{k_1} th antenna of the k_1th transmit sub-aperture is active. In matrix form, the new measurements can be expressed as

$$\boldsymbol{\xi}_{m_{k_1} n_{k_2}}^{(k_1,k_2)} = \boldsymbol{\Phi}_{m_{k_1} n_{k_2}}^{(k_1,k_2)} \boldsymbol{\Delta z}_{m_{k_1} n_{k_2}}^{(k_1,k_2)} = \boldsymbol{\Phi}_{m_{k_1} n_{k_2}}^{(k_1,k_2)} \boldsymbol{\Psi}_{m_{k_1} n_{k_2}}^{(k_1,k_2)} \boldsymbol{\delta\sigma}^{(k_1,k_2)} \tag{22}$$

where $\boldsymbol{\Phi}_{m_{k_1} n_{k_2}}^{(k_1,k_2)}$ is an $L \times K$ measurement matrix corresponding to the n_{k_2} th antenna position in the k_2th receive sub-aperture and the m_{k_1} th antenna in the k_1th transmit sub-aperture. Given $\boldsymbol{\xi}_{m_{k_1} n_{k_2}}^{(k_1,k_2)}$ for $m_{k_1}=0,1,\ldots,\lceil M/K_1 \rceil - 1$, $n_{k_2} = 0,1,\ldots,\lceil N/K_2 \rceil - 1$, we can recover $\boldsymbol{\delta\sigma}^{(k_1,k_2)}$ by solving the following equation:

$$\begin{aligned}\boldsymbol{\delta\hat{\sigma}}^{(k_1,k_2)} &= \arg\min_{\boldsymbol{\alpha}} \|\boldsymbol{\alpha}\|_1 \quad \text{subject to} \\ \boldsymbol{\Phi}^{(k_1,k_2)} \boldsymbol{\Psi}^{(k_1,k_2)} \boldsymbol{\alpha} &\approx \boldsymbol{\xi}^{(k_1,k_2)} \end{aligned} \tag{23}$$

where (24), shown at the bottom of the page. Once the sub-images $\boldsymbol{\delta\hat{\sigma}}^{(k_1,k_2)}$ corresponding to all K_1 transmit and K_2 receive sub-apertures have been reconstructed, the composite image $\boldsymbol{\delta\hat{\sigma}}$ can be formed as

$$[\boldsymbol{\delta\hat{\sigma}}]_q = \arg\max_{k_1,k_2} \left| \left[\boldsymbol{\delta\hat{\sigma}}^{(k_1,k_2)} \right]_q \right| \tag{25}$$

where $[\boldsymbol{\delta\hat{\sigma}}]_q$ and $[\boldsymbol{\delta\hat{\sigma}}^{(k_1,k_2)}]_q$ denote the qth pixel of the composite image and the sub-image corresponding to the k_1th transmit and k_2th receive sub-apertures, respectively. Alternatively, the sub-aperture image combining can be achieved using

$$[\boldsymbol{\delta\hat{\sigma}}]_q = \sum_{k_1=1}^{K_1} \sum_{k_2=1}^{K_2} \left| \left[\boldsymbol{\delta\hat{\sigma}}^{(k_1,k_2)} \right]_q \right|. \tag{26}$$

The expression in (25) performs a nonlinear combination of the pixel magnitudes of the sub-images, whereas (26) forms the composite image through a linear combination of the sub-aperture images.

It is noted that the model and reconstruction approach presented here for short sudden movements of the human target are also applicable to translational motion for the case when two consecutive measurements are used for CD. In this case, similar to short sudden movements, only a small part of the body moves; however, unlike the short movements, the body

$$\begin{aligned}\boldsymbol{\Psi}^{(k_1,k_2)} &= \left[\left(\boldsymbol{\Psi}_{00}^{(k_1,k_2)}\right)^T \left(\boldsymbol{\Psi}_{01}^{(k_1,k_2)}\right)^T \cdots \left(\boldsymbol{\Psi}_{\lceil \frac{M}{K_1} \rceil - 1, \lceil \frac{N}{K_2} \rceil - 1}^{(k_1,k_2)}\right)^T \right]^T \\ \boldsymbol{\Phi}^{(k_1,k_2)} &= \operatorname{diag}\left(\boldsymbol{\Phi}_{00}^{(k_1,k_2)} \; \boldsymbol{\Phi}_{01}^{(k_1,k_2)} \; \cdots \; \boldsymbol{\Phi}_{\lceil \frac{M}{K_1} \rceil - 1, \lceil \frac{N}{K_2} \rceil - 1}^{(k_1,k_2)} \right) \\ \boldsymbol{\xi}^{(k_1,k_2)} &= \left[\left(\boldsymbol{\xi}_{00}^{(k_1,k_2)}\right)^T \left(\boldsymbol{\xi}_{01}^{(k_1,k_2)}\right)^T \cdots \left(\boldsymbol{\xi}_{\lceil \frac{M}{K_1} \rceil - 1, \lceil \frac{N}{K_2} \rceil - 1}^{(k_1,k_2)}\right)^T \right]^T \end{aligned} \tag{24}$$

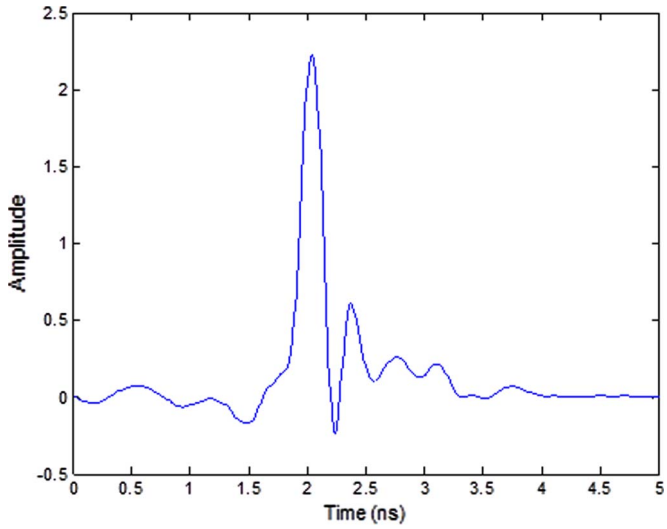

Fig. 1. Wideband pulse used for imaging.

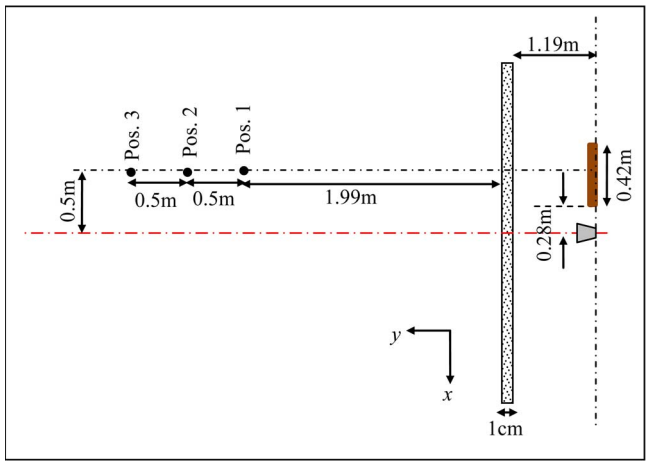

Fig. 2. Scene layout for the target undergoing translational motion.

part may move into the next resolution cell. This will lead to changes in scene reflectivity for both resolution cells.

V. Experimental Results

A through-the-wall wideband pulsed radar system was used for real data collection in the Radar Imaging Lab at Villanova University. The system uses a 0.7-ns pulse, shown in Fig. 1, for scene interrogation. The pulse is up-converted to 3 GHz for transmission and down-converted to base band through in-phase and quadrature demodulation on reception. The system operational bandwidth from 1.5–4.5 GHz provides a range resolution of 5 cm. The peak transmit power is 25 dBm. Transmission is through a single horn antenna, model BAE-H1479, with an operational bandwidth from 1 to 12.4 GHz, which is mounted on a tripod. An eight-element line array of Vivaldi elements with an inter-element spacing of 0.06 m, is used as the receiver and is placed to the right of the transmit antenna. The center-to-center separation between the transmitter and the leftmost receive antenna is 0.28 m, as shown in Fig. 2. A 3.65 m $\times$ 2.6 m wall segment was constructed utilizing 1-cm-thick cement board on a 2-by-4 wood stud frame. The transmit antenna and the receive array were at a standoff distance of 1.19 m from the wall. The pulse repetition frequency (PRF) is 10 MHz, providing an unambiguous range of 15 m, which is roughly three times the length of the room being imaged. Despite the high PRF, the system refresh rate is 100 Hz. This is because 1) equivalent time sampling is used [36], and 2) instead of simultaneous reception, the receive array elements are accessed sequentially through a multiplexer.

In order to illustrate the performance of the sparsity-driven CD scheme under both translational and sudden short human motions, two different experiments were considered. In the first experiment, a person walked away from the wall in an empty room (the back and the side walls were covered with RF absorbing material) along a straight line path. The path is located 0.5 m to the right of the center of the scene, as shown in Fig. 2. The data collection started with the target at position 1 and ended after the target reached position 3,

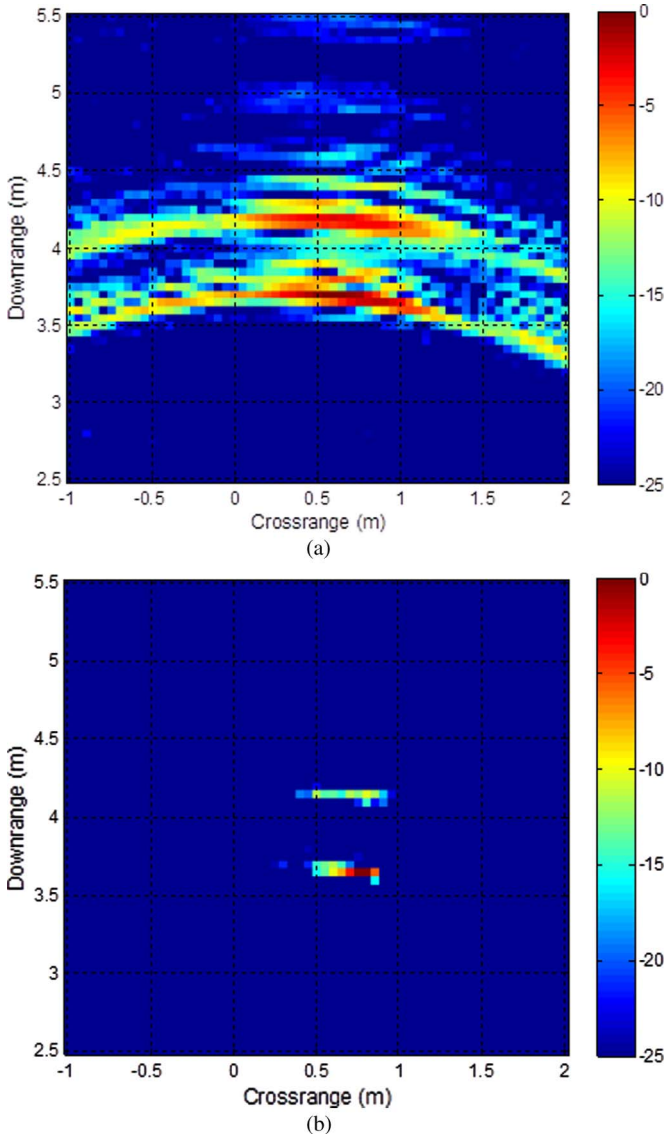

Fig. 3. (a) Back projection-based CD image using the full data set. (b) Sparsity-based CD image using 5% of the data volume, averaged over 100 trials.

with the target pausing at each position along the trajectory for a second. Consider the data frames corresponding to the target at position 2 and position 3. Each frame consists of 20 pulses, which are coherently integrated to improve the signal-to-noise ratio. The imaging region (target space) is chosen to be 3 m $\times$ 3 m, centered at (0.5 m, 4 m), and divided into 61 $\times$ 61 grid points in cross range and downrange, resulting in 3721 unknowns. The space-time response of the target space consists of 8 $\times$ 1536 space-time measurements. Fig. 3(a) shows the back projection-based CD image of the scene using all 8 $\times$ 1536 data points. In this figure and all subsequent figures in this section, we plot the image intensity with the maximum intensity value in each image normalized to 0 dB. We observe that, as the human changed its range gate position during the time elapsed between the two data acquisitions, it presents itself as two targets in the image and is correctly localized at both of its positions.

For sparsity-based CD, only 5% of the 1536 time samples are randomly selected at each of the eight receive antenna locations, resulting in 8 $\times$ 77 space-time measured data. More specifically, the 77 time samples at each receive location were obtained as the product of the 1536 point time-domain response with a 77 $\times$ 1536 measurement matrix, whose elements are randomly chosen ± 1 values with a probability of 1/2. According to CS theory, an r-sparse target space with Q unknowns can be recovered from $O(r\log(Q))$ measurements [37]. The human target roughly extended 0.5 m in cross range and 0.25 m in downrange, thereby occupying 10 $\times$ 5 grid points. Therefore, for the data set under consideration wherein the target presents itself as two targets after CD, the 8 $\times$ 77 measured data points exceed this requirement of $O(r\log(Q))$ measurements. We reconstructed the target space using sparsity-based CD with 5% data volume 100 times. For each trial, a different random measurement matrix was used to generate the reduced set of measurements, followed by sparsity-based scene reconstruction. For each of the 100 trials, we also computed the mutual coherence of the columns of the product of the measurement matrix $\mathbf{\Phi}$, with random ± 1 elemental values, and the $\mathbf{\Psi}$ matrix defined in (14). The average value of the mutual coherence of the corresponding product matrix is equal to 0.892. Fig. 3(b) shows the sparsity-based CD result, averaged over 100 trials. The higher the intensity of a grid point in this figure, the greater is the number of times that grid point was populated during the 100 reconstruction trials. We observe that, on average, the sparsity-based CD scheme detects and localizes the target accurately at both positions. Also, compared to the back projection-based result of Fig. 3(a), the image in Fig. 3(b) is less cluttered. The "cleaner" image is due to the fact that a sparse solution is enforced by the l_1 minimization in (13).

To further verify the performance of the sparsity-driven scheme, we computed the rate of successful reconstruction corresponding to the 100 trials for the translation motion. An image was regarded as a successful reconstruction if the pixel with the highest intensity was located within the extent of the target at the first (closer) position and if the second imaged target was populated with at least one pixel of significant intensity. Comparing the intensity of the two imaged targets in the back projected image, the significant pixel intensity was selected to be within 5 dB of the highest intensity. An example of a successful reconstruction is provided in Fig. 4. Based on these criteria, the successful recovery rate was determined to be 84%.

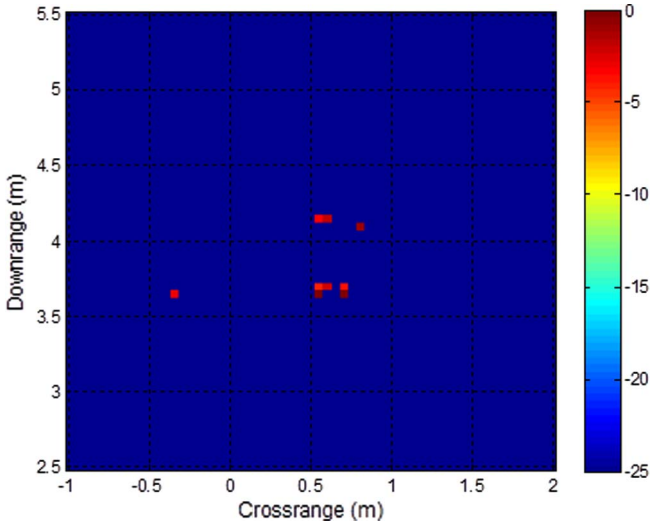

Fig. 4. Sparsity-based CD image for one of the trials under translational motion.

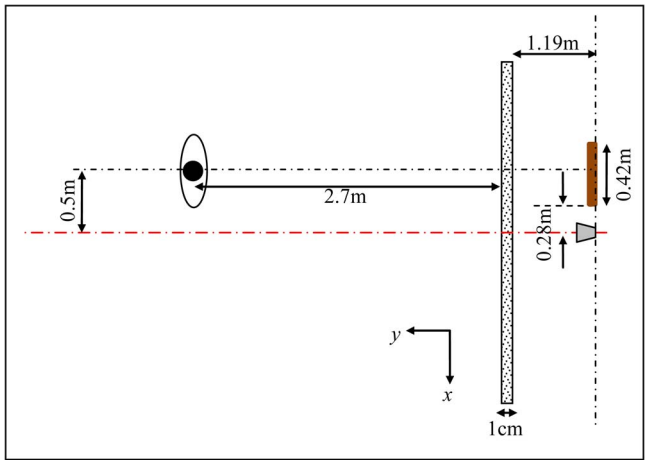

Fig. 5. Scene layout for the target undergoing sudden short movement.

Next, we collected data from a scene, consisting of a standing human facing the wall, located at 0.5 m cross range and at a downrange of 3.9 m from the radar, as shown in Fig. 5. The data was collected with the target initially looking straight at the wall and then suddenly lifting the head to look upward. As the person moved the head, there was also a slight movement of the shoulders and heaving of the chest. Two data frames of 20 pulses each, corresponding to the two head positions, were considered. The system parameters, the dimensions of the target space, the number of grid points, and the number of space-time measurements employed for the back projection-based and sparsity-based reconstructions are all the same as those for the translational motion example. The target space image obtained using the back projection-based CD with full data volume (after coherent integration) is shown in Fig. 6. We observe that the CD approach was able to detect the cumulative change in target reflectivity due to the head movement and

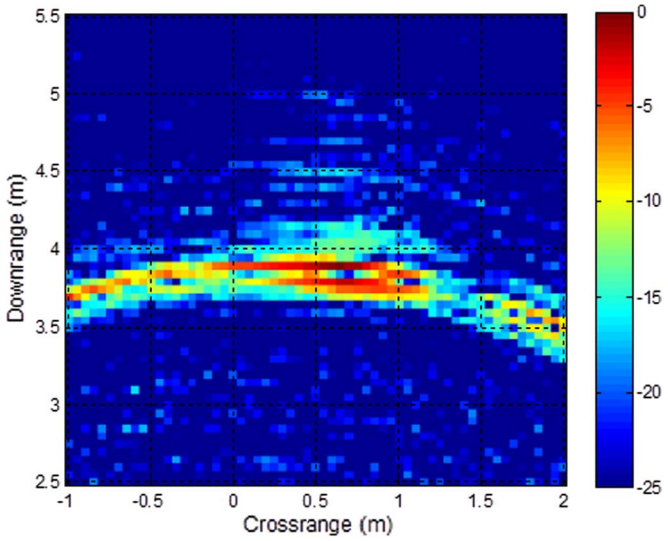

Fig. 6. Back projection based-CD image using full data volume for the target undergoing short sudden movement.

associated slight outward and upward movement of the chest as the target looked upward. Compared to the translational motion image of Fig. 3(a), the sudden short movement image is more cluttered. This is because the radar return is much weaker in this case due to a slight motion of only a small part of the body.

For the corresponding sparsity-based CD composite imaging results, we used two sub-apertures, each consisting of four receive antenna elements, and employed only 5% of the total data volume. That is, we used 77 time samples per antenna location within each of the sub-apertures. Similar to the translational motion example, we performed scene reconstruction 100 times, and the averaged target space images with the sub-images combined in accordance to (25) and (26) are provided in Fig. 7(a) and (b), respectively. We observe that, on average, the two sub-image combining approaches provide comparable performance, and the sparsity-based CD approach successfully detects and localizes the target undergoing short movement using much reduced data volume. For comparison, the sparsity-based scene reconstruction using the full receive array and 5% data volume, averaged over 100 trials, is also provided in Fig. 8. We note that although the non-composite image approach, on average, detects the presence of both the head and chest movements, the location of the highest intensity pixel is offset in downrange by about 5 cm. Despite this issue, the average performance of the non-composite scheme is reasonable compared to that of the composite imaging approaches. The reason being that the receive array is just 0.42 m in length, and the aspect angle variation across the array elements is no more than 6° for the considered target space. Thus, the isotropic scattering assumption is not violated through the use of the full receive array.

For the sudden movement case, we also computed the rate of successful reconstruction corresponding to the 100 trials for the sparsity-based composite image approaches. An image was regarded as a successful reconstruction if the pixel with the highest intensity was located within the extent of the target.

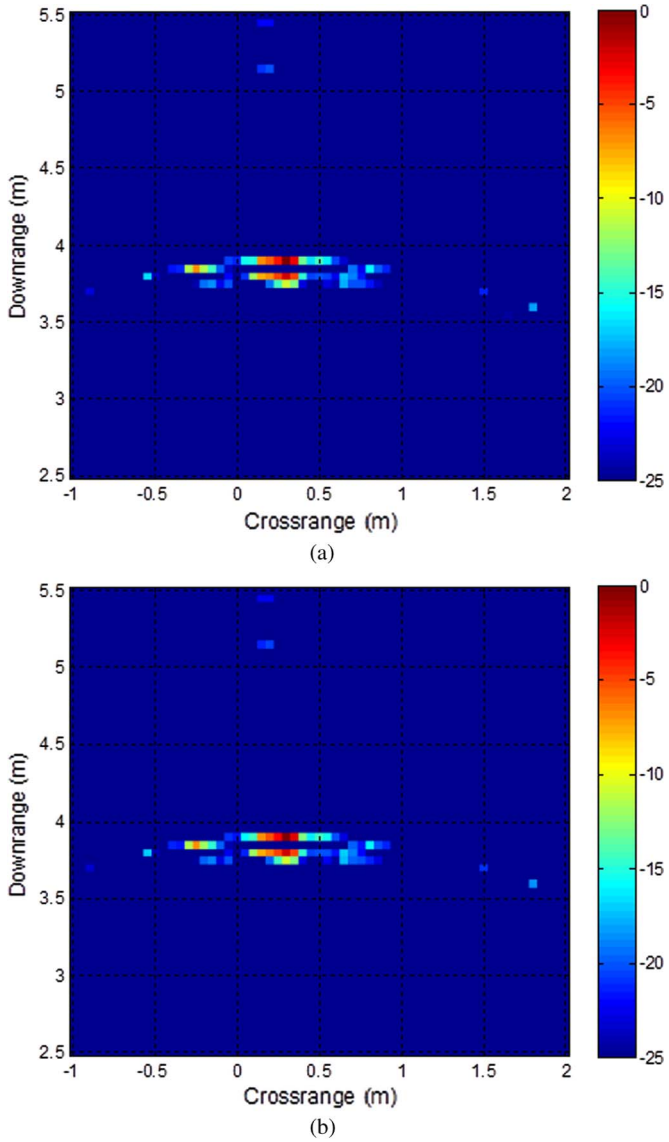

Fig. 7. Sparsity-based composite images with 5% data volume for the sub-image combining approach in (a) (25), and (b) (26). The images are the averages of 100 reconstructions.

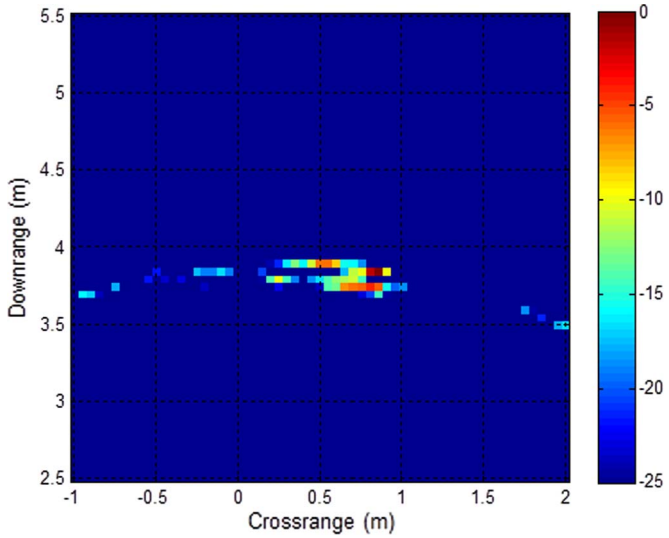

Fig. 8. Sparsity-based image using 5% data volume without partitioning the receive array into sub-apertures.

Based on this criterion, the respective successful recovery rates for the sub-image combination schemes of (25) and (26) were determined to be 75% and 73%.

VI. Conclusion

In this paper, we detected and localized moving humans behind walls and inside enclosed structures using an approach that combines sparsity-driven radar imaging and CD. Removal of stationary background via CD converts populated scenes to sparse scenes, whereby CS schemes can exploit full benefits of sparsity-driven imaging. Both translational motion and short sudden movements of the head, limbs, and/or torso were considered and appropriate CD models were developed for both motion types that allowed scene reconstruction within the CS framework. Examples of a human target undergoing translation motion and slight movement of the head behind a cement board wall were used to validate the developed models and to evaluate the performance of the proposed sparsity-driven CD scheme. Using pulsed radar operation, it was demonstrated that a sizable reduction in the data volume is achieved by the proposed approach without degradation in system performance.

It is noted that the work presented here only considered the sparsity of the target space and did not make any further assumptions about the support of the sparse solution during the reconstruction process. As the humans are extended targets, they appear as clusters in the through-the-wall images. As such, the corresponding sparse solution support has an underlying block structure [38], [39]. Future efforts will focus on exploiting this structured sparsity to further reduce the number of compressive measurements required for stable recovery.

References

[1] M. G. Amin, Ed., *Through-the-Wall Radar Imaging*. Boca Raton, FL: CRC Press, 2010.

[2] M. Amin and K. Sarabandi, Eds., "Special issue on remote sensing of building interior," *IEEE Trans. Geosci. Remote Sens.*, vol. 47, no. 5, pp. 1267–1268, May 2009.

[3] A. Martone, K. Ranney, and R. Innocenti, "Automatic through the wall detection of moving targets using low-frequency ultra-wideband radar," in *Proc. IEEE Int. Radar Conf.*, Washington, DC, May 2010, pp. 39–43.

[4] S. S. Ram and H. Ling, "Through-wall tracking of human movers using joint Doppler and array processing," *IEEE Geosci. Remote Sens. Lett.*, vol. 5, no. 3, pp. 537–541, Jul. 2008.

[5] M. Amin, Ed., "Special Issue on: Advances in indoor radar imaging," *J. Franklin Inst.*, vol. 345, no. 6, pp. 556–722, 2008.

[6] T. Dogaru and C. Le, "Validation of X patch computer models for human body radar signature," Appl. Res. Lab.–Univ. Texas, Austin, TX, US ARL Tech. Rep. ARL-TR-4403, Mar. 2008.

[7] C. P. Lai and R. M. Narayanan, "Through-wall imaging and characterization of human activity using ultrawideband (UWB) random noise radar," in *Proc. SPIE—Sens. C3I Technol. Homeland Security Homeland Defense*, May 2005, vol. 5778, pp. 186–195.

[8] S. S. Ram, Y. Li, A. Lin, and H. Ling, "Doppler-based detection and tracking of humans in indoor environments," *J. Franklin Inst.*, vol. 345, no. 6, pp. 679–699, Sep. 2008.

[9] T. Thayaparan, L. Stankovic, and I. Djurovic, "Micro-Doppler human signature detection and its application to gait recognition and indoor imaging," *J. Franklin Inst.*, vol. 345, no. 6, pp. 700–722, Sep. 2008.

[10] I. Orovic, S. Stankovic, and M. Amin, "A new approach for classification of human gait based on time-frequency feature representations," *Signal Process.*, vol. 91, no. 6, pp. 1448–1456, Jun. 2011.

[11] A. R. Hunt, "Use of a frequency-hopping radar for imaging and motion detection through walls," *IEEE Trans. Geosci. Remote Sens.*, vol. 47, no. 5, pp. 1402–1408, May 2009.

[12] N. Maaref, P. Millot, C. Pichot, and O. Picon, "A study of UWB FM-CW radar for the detection of human beings in motion inside a building," *IEEE Trans. Geosci. Remote Sens.*, vol. 47, no. 5, pp. 1297–1300, May 2009.

[13] T. S. Ralston, G. L. Charvat, and J. E. Peabody, "Real-time through-wall imaging using an ultrawideband multiple-input multiple-output (MIMO) phased array radar system," in *Proc. IEEE Intl. Symp. Phased Array Syst. Technol.*, Boston, MA, Oct. 2010, pp. 551–558.

[14] M. G. Amin and F. Ahmad, "Change detection analysis of humans moving behind walls," *IEEE Trans. Aerosp. Electron. Syst.*, to be published.

[15] F. Soldovieri, R. Solimene, and R. Pierri, "A simple strategy to detect changes in through the wall imaging," *Progr. Electromagn. Res. M*, vol. 7, pp. 1–13, 2009.

[16] J. Moulton, S. A. Kassam, F. Ahmad, M. G. Amin, and K. Yemelyanov, "Target and change detection in synthetic aperture radar sensing of urban structures," in *Proc. IEEE Radar Conf.*, Rome, Italy, May 2008.

[17] M. G. Amin, F. Ahmad, and W. Zhang, "A compressive sensing approach to moving target indication for urban sensing," in *Proc. IEEE Radar Conf*, Kansas City, MO, May 2011, pp. 1–6.

[18] R. Baraniuk and P. Steeghs, "Compressive radar imaging," in *Proc. IEEE Radar Conf.*, Waltham, MA, Apr. 2007, pp. 128–133.

[19] M. Herman and T. Strohmer, "High-resolution radar via compressive sensing," *IEEE Trans. Signal Process.*, vol. 57, no. 6, pp. 2275–2284, Jun. 2009.

[20] A. Gurbuz, J. McClellan, and W. Scott, Jr., "Compressive sensing for subsurface imaging using ground penetrating radar," *Signal Process.*, vol. 89, no. 10, pp. 1959–1972, Oct. 2009.

[21] L. C. Potter, E. Ertin, 1. T. Parker, and M. Cetin, "Sparsity and compressed sensing in radar imaging," *Proc. IEEE*, vol. 98, no. 6, pp. 1006–1020, Jun. 2010.

[22] Y. Yoon and M. G. Amin, "Compressed sensing technique for high-resolution radar imaging," in *Proc. SPIE*, 2008, vol. 6968, pp. 696 81A-1–696 81A-10.

[23] Q. Huang, L. Qu, B. Wu, and G. Fang, "UWB through-wall imaging based on compressive sensing," *IEEE Trans. Geosci. Remote Sens.*, vol. 48, no. 3, pp. 1408–1415, Mar. 2010.

[24] M. Leigsnering, C. Debes, and A. M. Zoubir, "Compressive sensing in through-the-wall radar imaging," in *Proc. IEEE Int. Conf. Acoust., Speech, Signal Process.*, Prague, Czech Republic, May 2011, pp. 4008–4011.

[25] K. Ranney, A. Martone, L. Nguyen, B. Stanton, M. Ressler, D. Wong, F. Koenig, C. Tran, G. Kirose, G. Smith, K. Kappra, and J. Sichina, "Recent MTI experiments using ARL's Synchronous Impulse Reconstruction (SIRE) radar," in *Proc. SPIE—Radar Sensor Technology XIV*, Apr. 2008, vol. 6947, pp. 694 708-1–694 708-9.

[26] P. Sévigny, D. J. DiFilippo, T. Laneve, B. Chan, J. Fournier, S. Roy, B. Ricard, and J. Maheux, "Concept of operation and preliminary experimental results of the DRDC through-wall SAR system," in *Proc. SPIE—Radar Sensor Technology XIV*, Apr. 2010, vol. 7669, pp. 766 907-1–766 907-11.

[27] F. Ahmad, Y. Zhang, and M. G. Amin, "Three-dimensional wideband beamforming for imaging through a single wall," *IEEE Geosci. Remote Sens. Lett.*, vol. 5, no. 2, pp. 176–179, Apr. 2008.

[28] M. G. Amin and F. Ahmad, "Wideband synthetic aperture beamforming for through-the-wall imaging," *IEEE Signal Process. Mag.*, vol. 25, no. 4, pp. 110–113, Jul. 2008.

[29] L. He, S. A. Kassam, F. Ahmad, and M. G. Amin, "Sparse multi-frequency waveform design for wideband imaging," in *Principles of Waveform Diversity and Design*, M. Wicks, E. Mokole, S. Blunt, R. Schneible, and V. Amuso, Eds. Raleigh, NC: SciTech Publ., 2010, pp. 922–938.

[30] X. X. Zhu and R. Bamler, "Tomographic SAR inversion by L_1-norm regularization—The compressive sensing approach," *IEEE Trans. Geosci. Remote Sens.*, vol. 48, no. 10, pp. 3839–3846, Oct. 2010.

[31] E. Candes, J. Romberg, and T. Tao, "Stable signal recovery from incomplete and inaccurate measurements," *Commun. Pure Appl. Math.*, vol. 59, no. 8, pp. 1207–1223, Aug. 2006.

[32] R. Baraniuk, M. Davenport, R. DeVore, and M. Wakin, "A simple proof of the restricted isometry property for random matrices," *Constructive Approx.*, vol. 28, no. 3, pp. 253–263, Dec. 2008.

[33] D. Needell and J. A. Tropp, "CoSaMP: Iterative signal recovery from incomplete and inaccurate samples," *Appl. Comput. Harmon. Anal.*, vol. 26, no. 3, pp. 301–321, May 2009.

[34] R. Tibshirani, "Regression shrinkage and selection via the LASSO," *J. R. Stat. Soc. B.*, vol. 58, no. 1, pp. 267–288, 1996.

[35] M. Cetin and R. L. Moses, "SAR imaging from partial-aperture data with frequency-band omissions," in *Proc. SPIE*, 2005, vol. 5808, pp. 32–43.
[36] Y. Yang and A. Fathy, "Development and implementation of a real-time see-through-wall radar system based on FPGA," *IEEE Trans. Geosci. Remote Sens.*, vol. 47, no. 5, pp. 1270–1280, May 2009.
[37] M. T. Alonso, P. López-Dekker, and J. J. Mallorquí, "A novel strategy for radar imaging based on compressive sensing," *IEEE Trans. Geosci. Remote Sens.*, vol. 48, no. 12, pp. 4285–4295, Dec. 2010.
[38] R. G. Baraniuk, V. Cevher, M. F. Duarte, and C. Hegde, "Model-based compressive sensing," *IEEE Trans. Inf. Theory*, vol. 56, no. 4, pp. 1982–2001, Apr. 2010.
[39] V. Cevher, P. Indyk, C. Hegde, and R. G. Baraniuk, "Recovery of clustered sparse signalsfrom compressive measurements," in *Proc. 8th Int. Conf. Sampling Theory Appl.*, Marseille, France, May 2009.

Fauzia Ahmad (S'97–M'97–SM'06) received the M.S. degree in electrical engineering and the Ph.D. degree in electrical engineering, both from the University of Pennsylvania, Philadelphia, in 1996 and 1997, respectively.

From 1998 to 2000, she was an Assistant Professor in the College of Electrical and Mechanical Engineering, National University of Sciences and Technology, Pakistan. During 2000–2001, she served as an Assistant Professor at the Fizaia College of Information Technology, Pakistan. Since 2002, she has been with the Center for Advanced Communications, Villanova University, Villanova, PA, where she is now a Research Associate Professor and the Director of the Radar Imaging Lab.

Dr. Ahmad has over 100 journal and conference publications in the areas of radar imaging, radar signal processing, waveform design and diversity, compressive sensing, array signal processing, sensor networks, ultrasound imaging, and over-the-horizon radar.

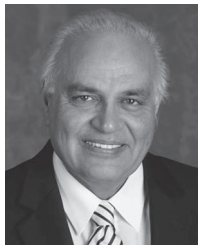

Moeness G. Amin (F'01) received the Ph.D. degree in electrical engineering from the University of Colorado, Boulder, in 1984.

He has been with the Faculty of the Department of Electrical and Computer Engineering at Villanova University, Villanova, PA, since 1985. In 2002, he became the Director of the Center for Advanced Communications, College of Engineering. He has over 450 journal and conference publications in the areas of wireless communications, time-frequency analysis, smart antennas, waveform design and diversity, interference cancellation in broadband communication platforms, anti-jam GPS, target localization and tracking, direction finding, channel diversity and equalization, ultrasound imaging and radar signal processing.

Dr. Amin is the Recipient of the 2009 Individual Technical Achievement Award from the European Association of Signal Processing, and the Recipient of the 2010 NATO Scientific Achievement Award. He is a Fellow of the International Society of Optical Engineering and a Fellow of the Institute of Engineering and Technology (IET). He is a Recipient of the IEEE Third Millennium Medal; Recipient of the Chief of Naval Research Challenge Award, 2010; Distinguished Lecturer of the IEEE Signal Processing Society, 2003–2004; Active Member of the Franklin Institute Committee on Science and the Arts; Recipient of Villanova University Outstanding Faculty Research Award, 1997; and the Recipient of the IEEE Philadelphia Section Award, 1997. He is a member of SPIE, EURASIP, ION, Eta Kappa Nu, Sigma Xi, and Phi Kappa Phi. He is a Recipient of seven best paper awards. Currenlty, he serves on the Overview Board of the IEEE TRANSACTIONS ON SIGNAL PROCESSING. He also serves on the Editorial Board of the EURASIP *Signal Processing Journal* and the Editorial Board of the *Signal Processing Magazine*. He was a Plenary Speaker at ICASSP 2010. He was the Special Session Co-Chair of the 2008 IEEE International Conference on Acoustics, Speech, and Signal Processing. He was the Technical Program Chair of the 2nd IEEE International Symposium on Signal Processing and Information Technology, 2002. He was the General and Organization Chair of the IEEE Workshop on Statistical Signal and Array Processing, 2000. He was the General and Organization Chair of the IEEE International Symposium on Time-Frequency and Time-Scale Analysis, 1994. He was an Associate Editor of the IEEE TRANSACTIONS ON SIGNAL PROCESSING during 1996–1998. He was a member of the IEEE Signal Processing Society Technical Committee on Signal Processing for Communications during 1998–2002. He was a member of the IEEE Signal Processing Society Technical Committee on Statistical Signal and Array Processing during 1995–1997. He was a Guest Editor of the *Journal of Franklin Institute* September-08 Special Issue on Advances in Indoor Radar Imaging. He was a Guest Editor of the IEEE TRANSACTIONS ON GEOSCIENCE AND REMOTE SENSING May-09 Special Issue on Remote Sensing of Building Interior, and a Guest Editor of the *IET Signal Processing* December-09 Special Issue on Time-Frequency Approach to Radar Detection, Imaging, and Classification.